JOURNAL OF AIRCRAFT
Vol. 36, No. 4, July–August 1999

Engineering Notes

ENGINEERING NOTES are short manuscripts describing new developments or important results of a preliminary nature. These Notes cannot exceed 6 manuscript pages and 3 figures; a page of text may be substituted for a figure and vice versa. After informal review by the editors, they may be published within a few months of the date of receipt. Style requirements are the same as for regular contributions (see inside back cover).

Divergence and Convergence of Iterative Static Aeroelastic Solutions

Thomas A. Zeiler*
University of Alabama, Tuscaloosa, Alabama 35487

Nomenclature

I = identity matrix
K = stiffness matrix
$\boldsymbol{P}$ = load vector
Q = generalized aerodynamic force coefficient matrix
$\bar{q}$ = dynamic pressure
$\bar{q}_{\text{div}}$ = divergence dynamic pressure
r_1, r_2 = relaxation factors
$\Delta \boldsymbol{u}$ = deflection vector
λ = eigenvalue

Introduction

CALCULATIONS of static aeroelastic response must sometimes be done iteratively. Although many standard aeroelastic analysis techniques use a linear-lifting-surface aerodynamic theory, permitting the calculation of generalized aerodynamic force (GAF) coefficients,[1] iteration is unavoidable if the aerodynamic model is nonlinear. In such a case, a set of GAF coefficients does not exist in general. However, if structural deflections are small, the increments in aerodynamic loads may be nearly linear functions of the deflections in the near vicinity of any nonlinear point.

It is of interest, then, to understand the convergence behavior of iterative static aeroelastic solutions. In particular, the influence of the static aeroelastic instability known as *divergence* can have a substantial effect on the convergence behavior of such iterations. Because the divergence condition may be known only from a linearized approximation, one needs to be alert to the possibility of convergence difficulties that may arise, how to recognize them, and how to overcome them. The present work addresses the convergence behavior of linear iterative static aeroelastic calculations for restrained structures on the premise that the linear case is of practical interest for nonlinear iterations, being illustrative at worst and locally applicable at best.

Development

The load–deflection relationship for a discretized model of a restrained structure (such as a finite element model) can be written

$$K \Delta \boldsymbol{u} = \boldsymbol{P} \tag{1}$$

For static aeroelastic problems, $\boldsymbol{P}$ is generally, though not exclusively, a vector of aerodynamic forces. The force vector is composed of the forces $\boldsymbol{P}_0$ created by the attitude and shape of the undeformed structure as well as those forces $\Delta \boldsymbol{P}$ arising from the deformation of the structure. For the linear case, a GAF matrix Q may be defined:

$$\Delta \boldsymbol{P} = \bar{q} Q \Delta \boldsymbol{u} \tag{2}$$

Then, the total loads are

$$\boldsymbol{P} = \boldsymbol{P}_0 + \Delta \boldsymbol{P} \tag{3}$$

Substituting Eqs. (2) and (3) into Eq. (1), solving for deflections, and resubstituting into Eq. (3),

$$\boldsymbol{P} = [I - \bar{q} Q K^{-1}]^{-1} \boldsymbol{P}_0 \tag{4}$$

If the aeroelastic stiffness matrix $[K - \bar{q} Q]$ is singular, then the structure is at a condition for aeroelastic divergence. The divergence dynamic pressure can be obtained for the linear equation (4) as the solution to an eigenvalue problem

$$\det[K - \bar{q}_{\text{div}} Q] = 0 \tag{5}$$

where the critical divergence dynamic pressure $\bar{q}_{\text{div}}$ is the lowest positive eigenvalue.

Linear Simulation of Iterative Static Aeroelastic Computation

The aeroelastic calculation is treated as if it were a case in which the structural computations and nonlinear aerodynamic calculations are loosely coupled. That is, the aerodynamic calculations are converged before the resulting loads are transferred to the structural model for deflection calculations. However, we use the linear expression for the aerodynamic loads and compare the iterated result with the exact result that is possible in the linear case, Eq. (4).

As before, consider an initial load distribution $\boldsymbol{P}_0$ that corresponds to the aerodynamic loads on the rigid structure. The total load, including the aeroelastic increment resulting from deflections caused by the initial loads $\boldsymbol{P}_0$, is

$$\boldsymbol{P}_1 = \boldsymbol{P}_0 + \Delta \boldsymbol{P}_1 = [I + \bar{q} Q K^{-1}] \boldsymbol{P}_0 \tag{6}$$

Then, the second iteration proceeds using $\boldsymbol{P}_1$ to determine new increments in deflection and resulting load:

$$\boldsymbol{P}_2 = \boldsymbol{P}_0 + \Delta \boldsymbol{P}_2 = [I + [\bar{q} Q K^{-1}] + [\bar{q} Q K^{-1}]^2] \boldsymbol{P}_0 \tag{7}$$

A pattern emerges such that, after the nth iteration, the load vector is

$$\boldsymbol{P}_n = [I + [\bar{q} Q K^{-1}] + [\bar{q} Q K^{-1}]^2 + \cdots + [\bar{q} Q K^{-1}]^n] \boldsymbol{P}_0 = \sum_{i=0}^{n} [\bar{q} Q K^{-1}]^i \boldsymbol{P}_0 \tag{8}$$

In the proper circumstances, this series should converge to the exact solution, Eq. (4):

$$\lim_{n \to \infty} \sum_{i=0}^{n} [\bar{q} Q K^{-1}]^i \boldsymbol{P}_0 = [I - \bar{q} Q K^{-1}]^{-1} \boldsymbol{P}_0 \tag{9}$$

Received 17 February 1997; revision received 15 April 1998; accepted for publication 10 August 1998.

*Assistant Professor, Aerospace Engineering and Mechanics Department. Senior Member AIAA.

The series on the left-hand side of Eq. (9) is a geometric series in the matrix $\bar{q}QK^{-1}$. A scalar geometric series converges if the magnitude of the scalar is less than unity.[2] For a geometric series in the matrix A, consider

$$\lim_{n\to\infty}\sum_{i=0}^{n} A^i \boldsymbol{u} \tag{10}$$

where $\boldsymbol{u}$ is some vector. It can be shown that convergence of the matrix geometric series requires convergence of a set of scalar geometric series, where the scalars are the eigenvalues of the matrix A. Therefore, for the present aeroelastic problem, the eigenvalues of the matrix $[\bar{q}QK^{-1}]$ must be less than unity for the matrix series in Eq. (9) to converge. It can be shown that the matrix geometric series should converge as

$$\lim_{n\to\infty}\sum_{i=0}^{n} A^i \boldsymbol{u} = [I - A]^{-1}\boldsymbol{u} \tag{11}$$

Thus the series in Eq. (9) does converge to the desired result if the magnitudes of the eigenvalues of the matrix $\bar{q}QK^{-1}$ are less than unity. This same matrix $\bar{q}QK^{-1}$ is also crucial in determining the divergence dynamic pressure. The eigenvalues of $\bar{q}QK^{-1}$ are obtained from

$$\det[\lambda I - \bar{q}QK^{-1}] = 0 \tag{12}$$

Applying the aeroelastic divergence criterion,

$$\det\left[I - \bar{q}_{\text{div}}QK^{-1}\right] = 0 \tag{13}$$

Rewriting the eigenvalue problem as

$$\det[I - (\bar{q}/\lambda)QK^{-1}] = 0 \tag{14}$$

It is seen immediately that

$$\lambda = \bar{q}/\bar{q}_{\text{div}} \tag{15}$$

Because the magnitude of λ must be less than unity for the series to converge,

$$\bar{q} < |\bar{q}_{\text{div}}| \tag{16}$$

A common practice is to apply relaxation factors to the intermediate results (either deflections or loads) in iterations to assist convergence.[3] One technique is to use a weighted average of the result $\boldsymbol{P}_{i-1}$ of the previous iteration and the result $\boldsymbol{P}'_i$ of the current iteration as a replacement for the current result in the next iteration,

$$\boldsymbol{P}_i = r_1\boldsymbol{P}_{i-1} + r_2\boldsymbol{P}'_i \tag{17}$$

It can be shown that, for the nth iteration,

$$\boldsymbol{P}_n = r_2\sum_{i=0}^{n-1}\left(r_1 I + r_2\bar{q}QK^{-1}\right)^i \boldsymbol{P}_0 + \left(r_1 I + r_2\bar{q}QK^{-1}\right)^n \boldsymbol{P}_0 \tag{18}$$

In the limit, the last term on the right-hand side will vanish if the magnitude of the eigenvalues of $r_1 I + r_2\bar{q}QK^{-1}$ are less than unity, which is required for convergence. Then, using the known converged limit of a matrix geometric series, Eq. (11),

$$r_2\lim_{n\to\infty}\sum_{i=0}^{n-1}\left(r_1 I + r_2\bar{q}QK^{-1}\right)^i \boldsymbol{P}_0 = r_2\left[I - \left(r_1 I + r_2\bar{q}QK^{-1}\right)\right]^{-1}\boldsymbol{P}_0 \tag{19}$$

If $r_1 + r_2 = 1$, then

$$r_2\left[I - \left(r_1 I + r_2\bar{q}QK^{-1}\right)\right]^{-1}\boldsymbol{P}_0 = \left[I - \bar{q}QK^{-1}\right]^{-1}\boldsymbol{P}_0 \tag{20}$$

is satisfied easily. Limits on the scalars r_1 and r_2 can be established by applying the condition that the magnitudes of the eigenvalues of $(r_1 I + r_2\bar{q}QK^{-1})$ must be less than unity for the series to converge. When this is used along with the aeroelastic divergence criterion, as before, and $r_1 + r_2 = 1$,

$$0 < r_2(1 - \bar{q}/\bar{q}_{\text{div}}) < 2 \tag{21}$$

The dependence of the relaxation factors upon the dynamic pressure ratio is depicted in Fig. 1. The shaded regions are valid values of the relaxation factors. Relaxation factors in the darkly shaded region are valid for all situations except for when the flight dynamic pressure is greater than the divergence dynamic pressure, but this condition is not of practical interest.

The effects of relaxation on the pitching moment convergence for an elastically mounted airfoil[4] are depicted in Fig. 2 for four possible relationships between flight and divergence dynamic pressures. No relaxation is done for $\bar{q} > \bar{q}_{\text{div}}$ because it is not of practical interest.

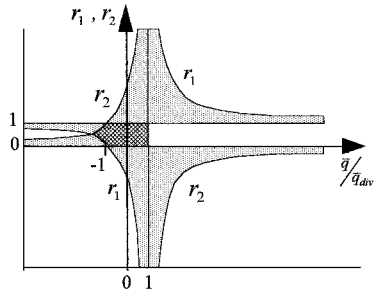

Fig. 1 Relaxation factors vs dynamic pressure ratio.

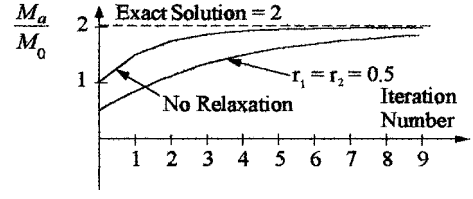

a) $\bar{q}_{\text{div}} > 0$ and $\bar{q} = \bar{q}_{\text{div}}/2$

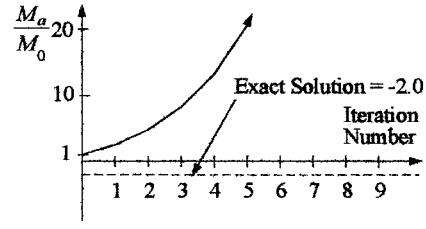

b) $\bar{q}_{\text{div}} > 0$ and $\bar{q} = 1.5\bar{q}_{\text{div}}$ (no relaxation)

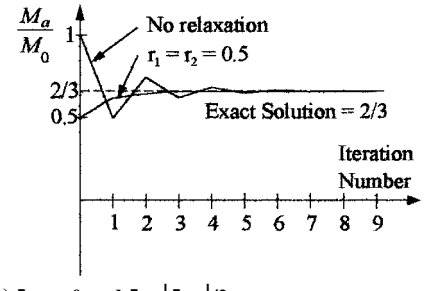

c) $\bar{q}_{\text{div}} < 0$ and $\bar{q} = |\bar{q}_{\text{div}}|/2$

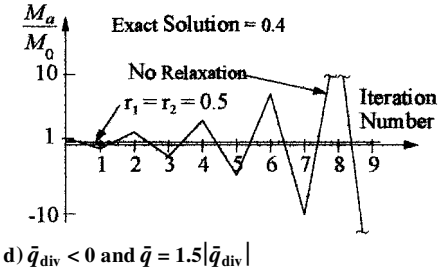

d) $\bar{q}_{\text{div}} < 0$ and $\bar{q} = 1.5|\bar{q}_{\text{div}}|$

Fig. 2 Iteration histories for two-dimensional airfoil.

The relaxation factors chosen (both equal to 0.5) dramatically improve the convergence of the two cases for which $\bar{q}_{\text{div}} < 0$. Although these factors worsen the convergence of the first case ($\bar{q}_{\text{div}} > \bar{q} > 0$), the iterations still converge.

Conclusions

The problem of convergence of iterative static aeroelastic solutions are discussed using a linear simulation. The intimate relationship of the flight and divergence dynamic pressures to the convergence behavior is derived and illustrated. Rigorous criteria are derived for selecting the relaxation factors to ensure convergence of the iterations for a linear system. Knowledge of the divergence speed for a linearized point in a nonlinear iteration should be of benefit to convergence of the nonlinear iteration.

References

[1]Rodden, W. P., and Love, J. R., "Equations of Motion of a Quasisteady Flight Vehicle Utilizing Restrained Static Aeroelastic Characteristics," *Journal of Aircraft*, Vol. 22, No. 9, 1985, pp. 802–809.

[2]Jolley, L. B. W., *Summation of Series*, Dover, New York, 1961, Series A, p. 2.

[3]Sensburg, O., Schweiger, J., Gödel, H., and Lotze, A., "Integration of Structural Optimization in the General Design Process for Aircraft," *Journal of Aircraft*, Vol. 31, No. 1, 1994, pp. 206–212.

[4]Bisplinghoff, R., Ashley, H., and Halfman, R., *Aeroelasticity*, Addison–Wesley, Reading, MA, 1955, Chap. 8.

Effect of a Splitter Plate on Transonic Wing Flow: A Numerical Study

G. Lombardi* and M. V. Salvetti†
University of Pisa, Pisa 56126, Italy

Introduction

In the experimental analysis of the flow around isolated wings, semimodels mounted on a sidewall are widely used. Indeed, this approach is very attractive, because supports are not needed, and, hence, the effects of the interference between models and supports are eliminated. On the other hand, the flow at the root of the semimodel is clearly different from that at the symmetry plane of the isolated wing, due to the effect of the sidewall boundary layer, as pointed out in Ref. 1 for a low-aspect-ratio wing. To reduce this effect, the model is commonly offset from the tunnel sidewall by means of a splitter plate. Nevertheless, even in this case, the splitter-plate boundary layer may significantly affect the experimental data. Furthermore, on a forward-swept wing in transonic flow, a strong shock wave is present in the wing root region; hence, significant interactions may occur between this shock wave and the sidewall boundary layer.

The motivation of the present study arises from the discrepancies observed at the wing root between experimental data and the results of a Navier–Stokes solver for the transonic flow around a forward-swept wing of high-aspect ratio.[2] Because these discrepancies are limited to the wing root region and good agreement is found on the remainder of the wing, a possible explanation is the influence of the sidewall boundary layer on the experimental data. Therefore, in the present paper, the effects of a sidewall boundary layer on the transonic flow around a forward-swept wing are numerically investigated.

Experimental Conditions and Numerical Method

The tests, carried out in the Medium Speed Wind Tunnel of the Council for Scientific and Industrial Research facilities, in South Africa, are described in Refs. 3 and 4. The wing model has zero twist and dihedral angles, a negative sweep angle ($\Lambda = -25$ deg, at one-quarter of the chord); aspect ratio $= 5.7$; taper ratio $= 0.4$; and NACA 0012 wing sections. The splitter plate used in the experiments is described in Ref. 4. Pressure measurements are available at 10 span stations and 32 chord points.[3] The measurement procedure and accuracy are described in Ref. 4. The data obtained in transonic regime ($M = 0.7$), at $Re \approx 2.8 \times 10^6$, based on the mean aerodynamic chord, are considered in this Note.

For the numerical solution of the Navier–Stokes equations, the commercial code RAMPANT[5] (developed by FLUENT) is used. Three-dimensional compressible Navier–Stokes or Reynolds-averaged Navier–Stokes equations can be solved. The numerical method is based on a finite volume formulation and is second-order accurate in space. Steady solutions are obtained by time-marching the equations with an explicit, multistage, Runge–Kutta scheme with multigrid convergence acceleration. The solution is considered to have reached convergence after a three-order-of-magnitude reduction of the rms residual for each of the conserved variables. A more detailed description of the numerical procedure can be found in Ref. 2.

In all of the simulations, the external boundary is represented by a cylinder of circular section, with a radius of 6.75 mean aerodynamic chords and a spanwise length of 2.5 wingspans, starting from the wing root. An analysis of the sensitivity to the dimensions of the computational domain was carried out, indicating that, for the domain used here, the influence of the external boundary conditions on the solution is negligible. All of the results presented next are obtained by solving the Reynolds-averaged Navier–Stokes equations with the standard k-ε model.

Analysis of the Results

In Fig. 1, the chordwise pressure distributions obtained in the numerical simulation, for the isolated wing at an angle of attack of 8 deg, are compared with the experimental data at two spanwise sections. The computational grid has approximately 175×10^3 cells. Figure 1b shows that at 40% of the semispan [$y/(b/2) = 0.4$], the numerical results are in good agreement with the experimental data. Conversely, at $y/(b/2) = 0.04$ (Fig. 1a), the position and intensity of the shock wave obtained numerically are completely different from those observed experimentally. Moreover, in the experiments, the shock wave induces a separation of the boundary layer; whereas in the numerical simulation, the boundary layer remains attached. Another simulation on a grid of approximately 300×10^3 cells, locally refined in the wing root region, showed the grid independence of the results.[2] As discussed previously, a possible explanation of the discrepancy between experimental data and numerical results is the presence in the experiments of a splitter plate that could affect the measurements, particularly in the region close to the wing root. To investigate this effect, a numerical simulation of the flow around the wing mounted on the splitter plate has also been carried out. The computational grid used in this simulation has approximately the same resolution as that used for the isolated wing (the total number of cells is $\cong 500 \times 10^3$).

The numerical chordwise pressure distributions, obtained at $y/(b/2) = 0.04$ and $y/(b/2) = 0.4$ in this simulation, are compared with those over the isolated wing and with the experimental data, in Figs. 2a and 2b, respectively.

Figure 2 shows that the splitter plate strongly affects the position and intensity of the shock wave near the wing root. In the simulation with the splitter plate, the shock wave moves upstream by about 10% of the local chord with respect to the isolated wing case, and the agreement with the experimental data is noticeably improved. Moreover, the boundary layer separates immediately behind the shock wave, as in the experiments. Nevertheless, the pressure

Received 17 February 1997; revision received 19 October 1998; accepted for publication 26 January 1999.

*Assistant Professor, Department of Aerospace Engineering. Member AIAA.

†Assistant Professor, Department of Aerospace Engineering.